

Evolution of cross-correlation and time lag of Cyg X-2 along the branches

Y.J. Lei¹, J.L. Qu¹, L.M. Song¹, C.M. Zhang^{1,2}, S. Zhang¹, F. Zhang¹, J.M. Wang¹, Z.B. Li¹, G.B. Zhang³

ABSTRACT

We report the detections of the anti-correlated soft and hard X-rays, and the time lags of \sim hecto-second from the neutron star low-mass X-ray binary Cyg X-2, a well-known Z-type luminous source. Both the anti-correlation and the positive correlation were detected during the low-intensity states, while only the latter showed up during high-intensity states. Comparing with the lower part of normal branch and flaring branch, more observations located on the horizontal and the upper normal branches are accompanied with the anti-correlation, implying the occurrence of the anti-correlation under circumstance of a low mass accretion rate. So far the anti-correlated hard lag of thousand-second timescale are only reported from the Galactic black hole candidates in their hard states. Here we provide the first evidence that a similar feature can also establish in a neutron-star system like Cyg X-2. Finally, the possible origins of the observed time lags are discussed under the current LMXB models.

Subject headings: accretion, accretion disk–binaries: close–stars: individual (Cygnus X-2)–X-rays: binaries

1. Introduction

The compact X-ray binary system hosts either a neutron star (NS) or a black hole (BH) candidate. Both systems show the similarity in their dependences on the X-ray luminosity

¹Particle Astrophysics Center, Institute of High Energy Physics, Chinese Academy of Sciences, Beijing 100049, P.R. China; leiyj@mail.ihep.ac.cn

²National Astronomical Observatories, Chinese Academy of Sciences, Beijing 100012, P.R. China

³Binhai College, Qingdao, Shandong, 266555, P.R. China

and spectral shape (van der Klis 1994a, 1994b, 2000; Belloni et al. 2002). The spectra of X-ray binaries are generally dominated by soft component, probably from the accretion disk and/or the surface of neutron star, and hard component from thermal Comptonization of soft photons in a hot plasma close to the compact object (Nowak et al. 1999b; Church 2001; Di Salvo et al. 2006b). Low-Mass X-ray Binary (LMXB) contains a companion with the mass $\lesssim 1 M_{\odot}$. NS LMXBs are divided into Z-type and Atoll-type according to the track shape in the color-color diagrams (CCDs), where the different position on the track correlates with the different timing behavior (Hasinger & van der Klis 1989; Hasinger 1990).

Cyg X-2 is a persistent LMXB, where the type-I X-ray bursts are detected, suggesting its compact star is a NS with a low magnetic field (e.g. Kahn & Grindlay 1984), and its mass is measured as $1.78 \pm 0.23 M_{\odot}$ (Orosz & Kuulkers 1999). The binary system has an evolved, late-type companion V1341 Cyg, with an orbital period of ~ 9.8 days (Cowley et al. 1979; Casares et al. 1998). Cyg X-2 is classified as a Z source according to its track on the CCD (Hasinger & van der Klis 1989; Hasinger 1990; van der Klis 2000), where the so-called horizontal branch (HB) is located at the top, and the normal branch (NB) and the flaring branch (FB) at the bottom. Along with the evolution of the source, it moves continuously on the Z-track, with each position related to the different mass accretion rate. The accretion rate reaches a minimum at the left end of the HB and a maximum at the right end of the FB (Hasinger & van der Klis 1989; Hasinger 1990). In addition, the quasi-periodic oscillations (QPOs) of Cyg X-2 are connected with the position on CCD as well: the frequency varies between ~ 15 and ~ 60 Hz on the HB and the upper part of the NB, and the low frequency about 5-7 Hz on the lower part of the NB (so-called NBOs) (Piraino et al. 2002; van der Klis 2000, 2006).

Although Z sources are the well-known LMXBs, the origin and evolution of the observed hard tails ($\gtrsim 30$ keV) are still remaining unclear. The hard power-law tails have been detected in the Z sources of e.g. Sco X-1 (Manchanda 2006), GX 5-1 (Asai et al. 1994), GX 17+2 (Di Salvo et al. 2000), GX 349+2 (Di Salvo et al. 2001), Cyg X-2 (Frontera et al. 1998), GX 340+0 (Lavagetto et al. 2004), and Cir X-1 (Iaria et al. 2001; Ding et al. 2003). Except for Sco X-1 whose hard tail does not show any clear correlation with the position of CCD as detected by the Rossi X-Ray Timing Explorer (*RXTE*) (D’Amico et al. 2001; Manchanda 2006), and could be correlated with the periods of radio flaring (Strickman & Barret 2000). for most of the others, the hard component appears to become weaker at the higher accretion rates. However, for Sco X-1, Di Salvo et al. (2006a) find that the flux of the power-law component slightly decreases when the source moves in the CCD from HB to NB, and becomes not significantly detected in FB with *INTEGRAL* and *RXTE*. The jets are also observed in the low magnetic field NS systems (Fender & Kuulkers 2001). For Cyg X-2, the hard tail is detected only in the HB spectra, which is consistent with the fact that the

radio flux is observed to have a maximum in HB (Hasinger et al. 1990; Di Salvo et al. 2002). Therefore, both the hard tail and radio emission could be produced by a jet (Penninx et al. 1988; Hasinger et al. 1990; Di Salvo et al. 2002). Such an accretion-ejection phenomena (Das & Chakrabarti 1999; Merier 2001) for the low magnetic NS systems is well addressed in the model of advection-dominated accretion flow by Narayan & Yi (1994).

Recently, an anti-correlated time lag ($\lesssim 2000s$) of the hard X-rays (20-50 keV) with respect to the soft X-rays (2-7 keV) is found in the hard state of some black hole X-ray binaries (BHXBs) (Choudhury & Rao 2004; Choudhury et al. 2005; Sriram et al. 2007). The timescale of the delay could be ascribed to the viscous timescale of matter flow in the optically thick accretion disk (Choudhury & Rao 2004). In addition, the outflow as a jet appears in the low-hard state of all BH sources and the truncated accretion disk also appears in low-hard state, which implies that the accretion disk emission is connected with the jet emission (Fender 2001; Choudhury et al. 2005). The purpose of this paper is to investigate whether the anti-correlation between the soft (2-5 keV) and hard (16-30 keV) X-rays exists as well in the NS LMXB system of Cyg X-2. The paper is organized as the follows. In section 2, the observations and data analysis of *RXTE* are introduced. In section 3, the results obtained on the QPO and the cross-correlation between the soft and hard X-rays are presented. Finally, in section 4 are the discussions and summary.

2. Observation and Data Reduction

The observations analyzed in this paper are from the Proportional Counter Array (PCA) on board the *RXTE* satellite. The PCA consists of 5 non-imaging, coaligned Xe multiwire proportional counter units (PCUs). The lightcurves are extracted with 4 ms resolution from the observations when PCUs were working and, accordingly, the power density spectra (PDS) are produced for QPO analysis. The data of the mode is B_2ms_16A_0_35_Q, where the time resolution is 2 ms (channel: 0-35¹). The PDS is produced by using the XRONOS tool of “*powspec*” (see Fig. 1).

For the analyses other than PDS, only PCU2 data are adopted due to the longest observational duration. For observations that containing segments longer than 2000 s, the lightcurves are extracted from the data of standard 2 mode, with bin size of 16 s, for estimating the cross-correlation via the XRONOS tool “*crosscor*”, between the soft X-rays (2-5

¹For the different gain epochs of RXTE, the energy channels 0-35 correspond to the different energy bands, the energy channels 0-35 of the five gain epochs correspond to 1.5-9.5 keV, 1.6-11 keV, 1.9-13 keV, 2-15 keV and 2-15 keV, respectively.

keV) and the hard X-rays (16-30 keV). With the FFT algorithm, “*crosscor*” computes the coefficient normalized by the square root of the number of good newbins in the lightcurves, and hence provides the cross covariance of the two lightcurves. The cross-correlation results are grouped into the positive (see Fig. 2), the ambiguous (see Fig. 3) and the anti-correlated (see Fig. 4). To investigate the accompanying time lag, we fit the cross-correlation curve with an inverted Gaussian function for the anti-correlated delay part of cross-correlations. As shown in Figure 4 is the anti-correlations between the soft and hard X-rays, accompanying with the pivoting spectra from the data with different hardness ratios, here the lightcurves of those with the count-rate ratio of 16-30 keV/2-5 keV $> 10\%$ than the average are regarded as the hard regions, and among the remaining $< 10\%$ than of the average as the soft regions.

For CCDs analysis, the soft and the hard colors are defined as well: as the count-rate ratio 4-6 keV/2-4 keV and 9.5-16 keV/6-9.5 keV (also see O’Brien et al. 2004), respectively, and the intensity is referred to the count-rate in the energy band 2-16 keV. The lightcurves are extracted from the 4-6 keV, 2-4 keV, 9.5-16 keV and 6-9.5 keV, with the background subtracted. The voltage settings of the PCUs on board *RXTE* are changed on three occasions, defining the five *RXTE* gain epochs. To correct the changes in effective area between the different *RXTE* gain epochs and the gain drifts within these epochs, we calculate the colors and intensity of the Crab Nebula with PCU2, which are supposed to be constant. We divide the obtained color points of each observation by the corresponding Crab values that are closest in time but within the same gain epoch (van Straaten et al. 2005). Figures 5-7 show the revised CCDs and HIDs with the bin size of 1024 s for different intensity states.

3. Results

3.1. Color-Color and Hardness-Intensity Diagrams

The intensity of Cyg X-2 is visible to vary on the time scales of days to months, and accordingly has the low-, medium- and high-intensity states. These states are associated with systematic changes in position and shape of the Z track in CCD and hardness-intensity diagrams (HID) (Kuulkers et al. 1996; Wijnands et al. 1996). In high level the Z pattern is shifted to higher overall intensity with respect to the pattern of a medium level. In the low intensity of Cyg X-2, we find several observations with peculiar CCDs and HIDs that are away from the general Z-pattern (see panels A and B in Fig. 5). The observations in panel A are from 28/29 September, 1997 and 16/17 December, 1999; in panel B from 23/24/26 December, 1999. Once Kuulkers et al. (1999) ascribed part of data (28/29 September, 1997) in the panel A to NB and FB. One sees in the CCD (the Panel B) that the data from 23/24/26 December, 1999 form a curved track, which seemly tracing the NB in the lower

part and the FB. But the corresponding evidences are not presented in the plot of HID.

Figure 6 shows the CCD well constructed from the observations of the dominated medium-intensity states and some low-intensity states. Unlikely shown in Figure 5, these observations of low-intensity state seem to be extensions towards lower intensity on the HB in HID and clearly show HB QPO. The CCD and HID of high-intensity states are shown in Figure 7. During the high-intensity level, the hard color of the HB is lower than that of the medium-intensity level. In the HID, the FB connects to the lower part of the NB, but this is not seen in the CCD. This implies that the intensity drops while the color remains the same.

3.2. Quasi-periodic Oscillation and Branch

While Cyg X-2 traces out a Z-track in CCD on timescales of days as a consequence of the change in the mass accretion rate, the morphology and position of the Z-track can vary on timescales of weeks to months (Kuulkers et al. 1996). Generally, the individual observation does not form a complete Z-track, and hence the branch information can not be obtained from the CCD only. However, it is well-known that the shape of the PDS and the centroid frequency of QPO evolve with the position in CCD for Z (Atoll) source (see e.g., Méndez & van der Klis 1999; Méndez 2000; Piraino et al. 2002). Therefore, we can estimate to which branch the lightcurve belongs, according to the CCD morphology, the PDS, and the centroid frequency of QPO.

For Cyg X-2, in general, QPOs with centroid frequency between ~ 15 and ~ 60 Hz are on the HB and upper part of the NB. Kuulkers et al. (1999) find a weak QPO signal at ~ 40 Hz from the observations on 28 September, 1997, and a weak noise component peaking around 6-7 Hz from the observations 29 September, 1997. Kuulkers et al. thus ascribe these observations to the NB and the FB. We calculate the PDS and find no obvious QPO signal from the observations on 16/17 December, 1999, implying a classification to the NB and the FB. The PDS shows only power-law noise component for the observations on 23/24 December and part observation of 26 December, 1999, and a QPO signal at $\sim 6-7$ Hz on other part of December 26.

For the observations in Figure 6 where the soft and hard X-rays are anti-correlated, the shape of PDS is power law and no NBO is found on the lower part of the NB and the FB. The HBOs is generally thought as the frame-dragging induced nodal frequency of tilt disk (Stella & Vietri 1998; Stella et al. 1999), the magnetoacoustic wave frequency (Titarchuk & Wood 2002), or the Alfvén wave oscillation (Zhang et al. 2007). Since we use the QPOs

for probing the branch location, and details on QPOs origin are beyond the content of this paper.

3.3. Cross-correlation between the Soft and Hard X-rays

We analyze the cross-correlation between the soft (2-5 keV) and the hard (16-30 keV) X-rays from all the observations available for Cyg X-2. As mentioned previously, there are three classes of the relationships according to the sign and the value of the derived correlation coefficient. In addition, observations showing simultaneously both positive and anti-correlation with different values of the time lag, as also classified as the ambiguous. Example to this is shown in Figure 3.

As shown in Figure 5, there are some special observations of Cyg X-2 during its low-intensity state. The soft and hard X-rays are mostly anti-correlated in the panel A of Figure 5, ambiguous in a few cases but not positive correlated. However, in panel B of Figure 5, only positive and ambiguous correlations show up.

The majority of the observations on Cyg X-2 are enclosed into the CCD plot (Fig. 6), which is divided into four regions. The data in region ‘I’ are on the vertical HB and HB, in region ‘II’ are on the HB and upper NB, in regions ‘III’/‘IV’ are on the low NB and FB. The hard and the soft X-rays are 26% anti-correlated and 28% positively correlated in region ‘I’; 14% anti-correlated and 51% positively correlated in region ‘II’; $\sim 7\%$ anti-correlated and $\sim 70\%$ positively correlated in the regions ‘III’/‘IV’ (Tab. 2). Obviously, there are more observations with anti-correlation in regions ‘I’ and ‘II’ than that in the regions ‘III’ and ‘IV’.

Figure 7 shows that the CCD and HID of the observations during the high-intensity state. From the right pattern of Figure 7, we can see that the intensity of the hard vertex (the transition between the HB and NB) is $> 2000 \text{ counts s}^{-1}$. The soft X-rays of all these observations are positively correlated with the hard X-rays.

Figure 4 shows the lightcurves of 2-5 keV and 16-30 keV and their cross-correlation functions for the observations owning the anti-correlations. Table 1 shows the ObsID, the time lag obtained with the FFT tool “*crosscor*”, and the FFT coefficient. For substantiating the correlation results from the FFT algorithm, we also estimate the Pearson coefficient using the Pearson’s test after correcting for the delay for each observation. The anti-correlation coefficients as derived with FFT and Pearson are consistent. Finally we have in these ObsIDs where the anti-correlations exist totally $\sim 20\%$ soft time lags, $\sim 60\%$ hard time lags and $\sim 20\%$ time lag not obvious. The timescale of soft lag is less than 200 s, and that of hard lag

is less than 400 s.

In addition, for the observations having anti-correlation, we show the spectral evolution in Figure 4, where the two spectra correspond to the soft and hard regions of the lightcurves, respectively. All the spectra present the pivoting in the energies 5-16 keV, further substantiating the existence of the anti-correlation between the soft and hard X-rays. Moreover, we also have tested all the observations of showing the positive correlation, and do not find pivoting in the spectral evolution, for instance in the ObsID 90030-01-32-00 as shown in Figure 2. For the ambiguous cases, the spectral pivoting of some observations exists, but is not obvious.

We also investigate on the cross-correlation on each individual observational segment of continuous data for those ObsIDs with anti-correlations detected. We find that, for each individual interval, some observations own the persistent anti-correlations, while some others have both the positive and anti-correlations. If we get rid of the observations that the cross-correlation functions of each individual interval of continuous data are not same, the distribution of anti-correlation is not affected. In this paper, only long timescale of cross-correlation function is considered.

4. Discussion

We have analyzed all the data available from *RXTE* observations on the NS Cyg X-2, and detected the anti-correlation between the soft (2-5 keV) and hard X-rays (16-30 keV). We find that, during the low-intensity state of Cyg X-2, there exists different observations showing separately either the anti-correlation or the positive correlation. These observations are located on the NB and FB in the CCD. But for the majority of the observations, the fraction of the observations with anti-correlation in HB and upper part of NB are larger than that in low part of NB and FB. During the high-intensity state only positive correlation is detected. Specially, during the FB of high-intensity state, the intensities decrease, but the colors remain the same.

The pivoting of the wide-band X-ray spectrum is also detected in all the observation with anti-correlation. The mass accretion rate of individual Z source increases along HB, NB and FB (van der Klis 2000; 2006). We discuss only the result in Figure 6 where most observations are included. The anti-correlation between the soft and hard X-rays is mostly found on the HB and upper parts of NB, which suggest that the anti-correlation could be associated with the low mass accretion rate. In the low-hard state of BHXBs, an anti-correlation of the soft (2-7 keV) and hard X-rays (20-50 keV) is detected, which suggests the

existence of a truncated accretion disk (Choudhury et al. 2005). At low accretion rates, the disk is truncated far away from the compact object and the X-ray spectrum is dominated by a thermal Compton spectrum. With the increase of the accretion rate, the location of the disk truncation moves in, resulting in the Comptonizing cloud to decrease as well as the amount of seed thermal photons to increase, which cools the Comptonizing cloud more efficiently, giving rise to the anti-correlation of hard and soft X-rays and the pivoting of the wide-band X-ray spectrum (Choudhury et al. 2005).

The timescale of this anti-correlated hard X-ray time lag is about thousand seconds in BHXBs, which is explained to be attributed to the viscous timescale of the matter flow in the radiation pressure dominated optically thick accretion disk (Choudhury & Rao 2004), i.e., the influence by the matter flow propagates from the outer disk (soft photon region) to the innermost disk (hard photon region). Our results show that, for NS LMXB Cyg X-2, the anti-correlated hard X-ray time lag is about several hundred seconds. It is considered that the hard X-ray emission could come from the Comptonizing of the soft seed photons for X-ray binary system. For BHXBs, the soft seed photons are produced from the accretion disk. However, for NS systems, the soft seed photons are produced from the surface of NS and/or the accretion disk, and the Comptonizing cloud might be a hot corona, a hot flared inner disk, or even the boundary layer between the NS and accretion disk if it is sufficiently thin and hot (also see Popham & Sunyaev 2001). If the soft seed photon comes from the NS surface, the hard photons come from the inverse Compton scattering of soft photons by hot electrons, and a hard lag of this Compton process is expected with timescale of about < 1 s (Hasinger 1987; van der Klis et al. 1987; Nowak et al. 1999a). If the soft X-rays come from the cool and dense blob, with the blob spiraling inward, it emits the soft X-ray radiation that is Comptonized in an hot and dense corona, which results in Comptonized X-ray spectrum to be harder with time, causing the hard time lags of timescale ~ 1 s (Böttcher & Liang 1999). Therefore, the above-mentioned models should be ruled out as the possible mechanisms for the several hundred-second time lags, and our results suggest that the hecto-second time lag should be produced by other mechanisms.

The timescale of the anti-correlated hard X-ray time lag is comparative to the viscous timescale of the compact systems, therefore, Choudhury and Rao (2004) ascribe the time lag of BH system to the viscous timescale of the matter flow in the radiation pressure dominated optically thick accretion disk. Assuming that the soft seed photons of Cyg X-2 come from the accretion disk, the viscous time t_{vis} in the disk can be calculated by

$$t_{vis} = 30\alpha^{-1}M^{-1/2}R^{7/2}\dot{M}^{-2}s$$

where α is the viscosity parameter in units of 0.01, M is the mass of the compact object in solar mass, R is the radial location in the accretion disk in units of 10^7 cm, \dot{M} is the mass

accretion rate in units of 10^{18} g/s (see Fender & Belloni 2004). For Cyg X-2, taking $\alpha = 1$, $M = 1.78$ and $\dot{M} = 1.3$ ($\sim 2 \times 10^{-8} M_{\odot} \text{ yr}^{-1}$, see Smale 1998), we get $R \sim 1.8$ for a viscous timescale of ~ 100 s. Thus, the observed delay will infer the location of the truncation of ~ 18 NS radius. Choudhury & Rao (2004) obtain the location of the disk truncation of ~ 25 Schwarzschild radius for the BHXB Cyg X-3. Table 1 shows the locations of the truncation of every ObsID with anti-correlated hard X-rays time lag, by assuming $\alpha = 1$ and $\dot{M} = 1.3$. The results of Table 1 show the locations of the truncation are not evolutionary along the branches. However, unlikely the BH binaries, for the Z sources, the X-ray intensity may not be proportional to \dot{M} , or \dot{M} can not be estimated accurately. In addition, the viscosity parameter α could be different for the different position of Z-track. Therefore, we can not obtain the locations of the truncation accurately, maybe, different from the results of Table 1, the locations of the truncations are evolutionary along Z-track.

The above model can explain the anti-correlated hard X-ray lag, however, it can not explain the anti-correlated soft X-ray lag. The anti-correlated soft X-ray lag (< 200 s) is also detected in Cyg X-2, whose timescale is comparative to the viscous timescale. If a fluctuation produced from the innermost accretion disk could propagate to the outer accretion disk and modulates the soft X-ray emission regions, the soft lag is about to be explained. It is possible to produce such a fluctuation, since the model by Li et al. (2007) provides a probability for it, which ascribes the accretion disk to be thermally unstable and to exhibit the limit-cycle behavior (see also e.g. Kato et al. 1998). In the cycle process, the expansion wave in the innermost disk can be formed and moves outward with time, which perturbs the outer material, modulating the soft X-ray emission, and resulting in the soft X-ray lag, and the timescale is several hundred seconds.

The anti-correlation in BH binary systems implies that the geometric structure of the disk-jet could be connected with a truncated disk (Choudhury & Rao 2004; Choudhury et al. 2005). The truncated accretion disk could occur in the low-hard state where the outflow in the form of a jet is present. In NS LMXB Cyg X-2, a hard power-low tail is significantly detected only in the HB spectra (Di Salvo et al. 2002). The strong non-thermal radio flares are observed in the HB and upper NB, and the source is radio quiet in the lower NB and FB (Hasinger et al. 1990). Therefore, the hard power-law component could be related with the radio flares, and the hard power-law component is related to the high-velocity electrons (probably from a jet) of producing the radio emission (Di Salvo et al. 2002). Our results show that in Cyg X-2 the anti-correlations mostly present in HB and upper NB, at where the hard power-law component and radio flares also occur.

The authors are grateful to the anonymous referee for the helpful comments. We are thankful for S.N. Zhang for the useful discussions. This research has made use of data

obtained through the high-energy Astrophysics Science Archive Research Center Online Service, provided by the NASA/Goddard Space Flight Center. We acknowledge the RXTE data teams at NASA/GSFC for their help. This work is subsidized by the Special Funds for Major State Basic Research Projects and by the Natural Science Foundation of China for support via NSFC 10473010, 10273010, 10773017, 10373013, 10733010, 10521001 and 10325313, CAS key project via KJCX2-YWT03.

REFERENCES

- Asai, K., Dotani, T., Mitsuda, K., Nagase, F., Kamado, Y., Kuulkers, E., & Breedon, L. M. 1994, PASJ, 46, 479
- Belloni, T., Psaltis, D., & van der Klis, M. 2002, ApJ, 572, 392
- Böttcher, M., & Liang, E. P. 1999, ApJ, 511, L37
- Casares, J., Charles, P. A., & Kuulkers, E. 1998, ApJ, 493, L39
- Choudhury, M., & Rao, A. R. 2004, ApJ, 616, L143
- Choudhury, M., Rao, A. R., Dasgupta, S., Pendharkar, J., Sriram, K., & Agrawal, V. K. 2005, ApJ, 631, 1072
- Church, M. J. 2001, Advances in Space Research, 28, 323
- Cowley, A. P., Crampton, D., & Hutchings, J. B. 1979, ApJ, 231, 539
- D’Amico, F., Heindl, W. A., Rothschild, R. E., & Gruber, D. E. 2001, ApJ, 547, L147
- Das, T. & Chakrabarti, S.K. 1999, Class & Quant. Gravity, 16, 3879
- Di Salvo, T., et al. 2000, ApJ, 544, L119
- Di Salvo, T., Robba, N. R., Iaria, R., Stella, L., Burderi, L., & Israel, G. L. 2001, ApJ, 554, 49
- Di Salvo, T., et al. 2002, A&A, 386, 535
- Di Salvo, T., et al. 2006a, ApJ, 649, L91
- Di Salvo, T., Iaria, R., Robba, N., & Burderi, L. 2006b, ChJAA, Suppl., 6, 183
- Ding, G. Q., Qu, J. L., & Li, T. P. 2003, ApJ, 596, L219

- Fender, R. P. 2001, MNRAS, 322, 31
- Fender, R.P. & Belloni, T. 2004, ARA&A, 42, 317-364
- Fender, R. P., & Kuulkers, E. 2001, MNRAS, 324, 923
- Frontera, F., et al. 1998, The Active X-ray Sky: Results from BeppoSAX and RXTE, 286
- Hasinger, G. 1987, IAU Symp. 125: The Origin and Evolution of Neutron Stars, 125, 333
- Hasinger, G., 1990, Reviews of Modern Astronomy, 3, 60
- Hasinger, G., & van der Klis, M. 1989, A&A, 225, 79
- Hasinger, G., van der Klis, M., Ebisawa, K., Dotani, T., & Mitsuda, K. 1990, A&A, 235, 131
- Iaria, R., Burderi, L., Di Salvo, T., La Barbera, A., & Robba, N. R. 2001, ApJ, 547, 412
- Kahn, S. M., & Grindlay, J. E. 1984, ApJ, 281, 826
- Kato, S., Fukue, J., & Mineshige, S. 1998, Black-Hole Accretion Disks (Kyoto: Kyoto Univ. Press)
- Kuulkers, E., van der Klis, M., & Vaughan, B. A. 1996, A&A, 311, 197
- Kuulkers, E., Wijnands, R., & van der Klis, M. 1999, MNRAS, 308, 485
- Lavagetto, G., Iaria, R., di Salvo, T., Burderi, L., Robba, N. R., Frontera, F., & Stella, L. 2004, Nuclear Physics B Proceedings Supplements, 132, 616
- Li, S.-L., Xue, L., & Lu, J.-F. 2007, ApJ, 666, 368
- Manchanda, R. K. 2006, Advances in Space Research, 37, 2139
- Meier, D. L. 2001, ApJ, 548, L9
- Méndez, M. 2000, Nuclear Physics B Proceedings Supplements, 80, 1516
- Méndez M, van der Klis M. 1999, ApJ, 517, L51
- Narayan, R., & Yi, I. 1994, ApJ, 428, L13
- Nowak, M. A., Wilms, J., & Dove, J. B. 1999a, ApJ, 517, 355

- Nowak, M. A., Wilms, J., Vaughan, B. A., Dove, J. B., & Begelman, M. C. 1999b, *ApJ*, 515, 726
- O’Brien, K., Horne, K., Gomer, R. H., Oke, J. B., & van der Klis, M. 2004, *MNRAS*, 350, 587
- Orosz, J. A., & Kuulkers, E. 1999, *MNRAS*, 305, 132
- Penninx, W., Lewin, W. H. G., Zijlstra, A. A., Mitsuda, K., & van Paradijs, J. 1988, *Nature*, 336, 146
- Piraino, S., Santangelo, A., & Kaaret, P. 2002, *ApJ*, 567, 1091
- Popham, R., & Sunyaev, R. 2001, *AIP Conf. Proc.* 599: X-ray Astronomy: Stellar Endpoints, AGN, and the Diffuse X-ray Background, 599, 870
- Smale, A. P. 1998, *ApJ*, 498, L141
- Strickman, M., & Barret, D. 2000, *American Institute of Physics Conference Series*, 510, 222
- Stella, L., & Vietri, M. 1998, *ApJ*, 492, L59
- Stella, L., Vietri, M., & Morsink, S. 1999, *ApJ*, 524, L63
- Sriram, K., Agrawal, V. K., Pendharkar, J. K., & Rao, A. R. 2007, *ApJ*, 661, 1055
- Titarchuk, L., & Wood, K.S. 2002, *ApJ*, 577, L23
- van der Klis, M. 1994a, *A&A*, 283, 469
- van der Klis, M. 1994b, *ApJS*, 92, 511
- van der Klis, M. 2000, *ARA&A*, 38, 717 (astro-ph/0001167)
- van der Klis, M. 2006, in *Compact stellar X-ray sources*, W.H.G. Lewin & M. van der Klis (eds.), Cambridge University Press, p. 39; (astro-ph/0410551).
- van der Klis, M., Hasinger, G., Stella, L., Langmeier, A., van Paradijs, J., & Lewin, W. H. G. 1987, *ApJ*, 319, L13
- van Straaten, S., van der Klis, M., & Wijnands, R. 2005, *ApJ*, 619, 455
- Wijnands, R. A. D., Kuulkers, E., & Smale, A. P. 1996, *ApJ*, 473, L45
- Zhang, C. M., Yin, H. X., & Zhao, Y. H. 2007, *PASP*, 119, 393

Table 1: **Details of ObsIDs which the anti-correlation of the hard and soft X-rays are detected.**

ObsID	Date Year-Month-Day	Location	Delay(Error) (s)	statistical coefficient		R ($10^7 cm$)
				FFT(Error)	Pearson (Null Probability)	
20057-01-01-000	1997-09-28	A/Fig. 5	-2(± 16)	-0.53(~ 0.01)	-0.51($< 10^{-5}$)	
20057-01-01-00	1997-09-28	A/Fig. 5	64(± 16)	-0.44(~ 0.02)	-0.43($< 10^{-5}$)	1.6
20057-01-01-010	1997-09-29	A/Fig. 5	-157(± 28)	-0.28(~ 0.01)	-0.29($< 10^{-5}$)	
40019-04-03-00	1999-12-16	A/Fig. 5	279(± 17)	-0.28(~ 0.01)	-0.18($< 10^{-5}$)	2.4
40019-04-04-000/00	1999-12-17	A/Fig. 5	74(± 13)	-0.57(~ 0.01)	-0.73($< 10^{-5}$)	1.6
40019-04-04-01	1999-12-17	A/Fig. 5	229(± 45)	-0.21(~ 0.01)	-0.15(4×10^{-2})	2.3
40017-02-16-02	1999-11-20	I/Fig. 6	-29(± 30)	-0.22(~ 0.02)	-0.24(3×10^{-3})	
40019-04-02-000/00	1999-09-23	I/Fig. 6	146(± 21)	-0.18(~ 0.01)	-0.34($< 10^{-5}$)	2.0
90030-01-46-00	2004-10-08	I/Fig. 6	348(± 18)	-0.24(~ 0.01)	-0.16(6×10^{-3})	2.4
30046-01-12-00	1998-09-25	I/Fig. 6	6(± 15)	-0.33(~ 0.01)	-0.38($< 10^{-5}$)	
90030-01-16-00	2004-05-13	I/Fig. 6	-37(± 32)	-0.37(~ 0.01)	-0.40($< 10^{-5}$)	
10066-01-01-00	1996-03-27	I/Fig. 6	-3(± 8)	-0.36(~ 0.01)	-0.39($< 10^{-5}$)	
90030-01-91-00	2005-12-25	I/Fig. 6	121(± 35)	-0.41(~ 0.02)	-0.39($< 10^{-5}$)	1.9
90030-01-95-00	2006-01-14	I/Fig. 6	11(± 30)	-0.16(~ 0.01)	-0.19($\sim 10^{-4}$)	
20053-04-01-03	1997-07-02	II/Fig. 6	-54(± 9)	-0.30(~ 0.01)	-0.32($< 10^{-5}$)	
90030-01-88-00	2005-12-10	II/Fig. 6	233(± 29)	-0.20(~ 0.01)	-0.20(4×10^{-4})	2.3
40017-02-18-00	1999-12-27	II/Fig. 6	255(± 28)	-0.49(~ 0.01)	-0.38($< 10^{-5}$)	2.3
91009-01-32-00	2005-08-04	II/Fig. 6	337(± 19)	-0.56(~ 0.01)	-0.55($< 10^{-5}$)	2.5
60417-01-02-00	2001-08-03	II/Fig. 6	-184(± 29)	-0.33(~ 0.03)	-0.19(4×10^{-2})	
90030-01-72-00	2005-02-13	II/Fig. 6	62(± 21)	-0.29(~ 0.01)	-0.23($\sim 10^{-3}$)	1.6
40017-02-07-00	1999-05-05	II/Fig. 6	376(± 25)	-0.39(~ 0.02)	-0.16($\sim 10^{-5}$)	2.6
90030-01-36-00	2004-08-20	II/Fig. 6	-35(± 25)	-0.30(~ 0.02)	-0.34($< 10^{-5}$)	
90030-01-31-00	2004-07-26	II/Fig. 6	277(± 70)	-0.36(~ 0.01)	-0.33($< 10^{-5}$)	1.8
30046-01-01-00	1998-07-15	II/Fig. 6	83(± 9)	-0.52(~ 0.01)	-0.51($< 10^{-5}$)	1.7
40021-02-01-00	2000-01-14	II/Fig. 6	178(± 15)	-0.38(~ 0.01)	-0.26($< 10^{-5}$)	2.1
30046-01-05-01	1998-08-10	III/Fig. 6	46(± 14)	-0.38(~ 0.01)	-0.41($< 10^{-5}$)	1.4
00029-04-01-00	1996-01-27	III/Fig. 6	17(± 29)	-0.40(~ 0.02)	-0.39($< 10^{-5}$)	
90022-08-02-00	2004-12-08	III/Fig. 6	124(± 39)	-0.40(~ 0.06)	-0.25(2×10^{-3})	1.9
90030-01-68-00	2005-01-24	III/Fig. 6	227(± 19)	-0.32(~ 0.01)	-0.22($\sim 10^{-5}$)	2.2
90030-01-67-00	2005-01-19	IV/Fig. 6	-41(± 16)	-0.50(~ 0.02)	-0.53($< 10^{-5}$)	

Note. — R is the locations of the truncation of the accretion disk, a viscous timescale of 100s is corresponding to 18 NS radius. 40019-04-02-000/00 is the observations of 40019-04-02-000 and 40019-04-02-00, and 40019-04-04-000/00 is the observations of 40019-04-04-000 and 40019-04-04-00.

Table 2: **The percent of positive and anti-correlation for each region of Figure 6.**

	I	II	III	IV
positive-correlation	28%	51%	76%	65%
anti-correlation	26%	14%	7%	7%
ambiguous	46%	35%	17%	28%

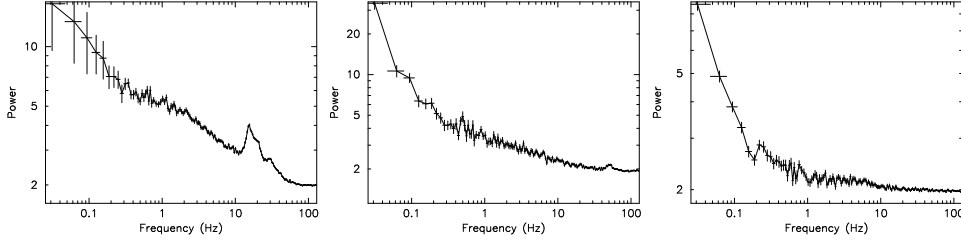


Fig. 1.— The left panel shows HBO with the centroid frequency $\sim 15\text{--}50$ Hz, the middle panel shows HBO with the centroid frequency $\gtrsim 50$ Hz, and the right one shows no QPO during the lower part of NB and FB.

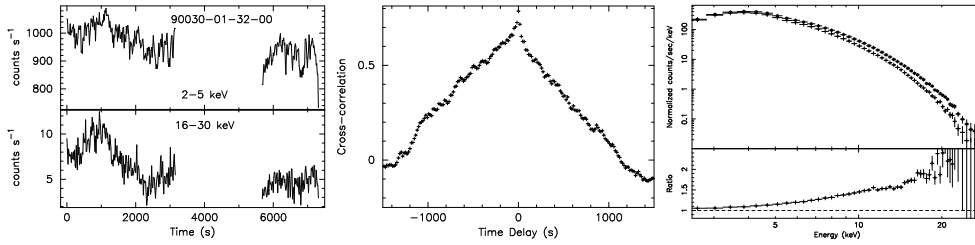


Fig. 2.— The left panel shows the lightcurves of ObsID 90030-01-32-00 and the middle panel shows the cross-correlation function where a typical positive correlation is observed. The right one shows the X-ray spectra of the ObsID for hard and soft regions of the lightcurve (upper) and the ratio of the hard and soft spectra (lower), where no pivoting is shown.

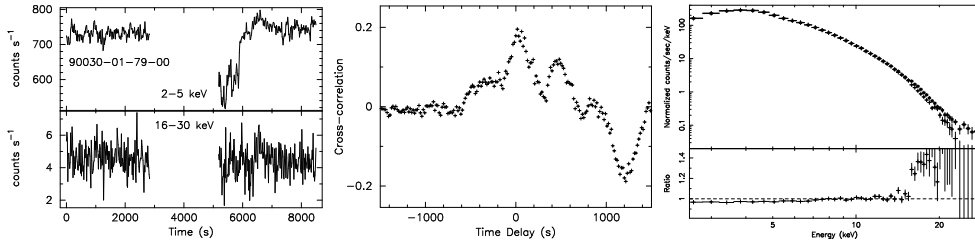


Fig. 3.— The left panel shows the lightcurves of ObsID 90030-01-79-00 and the middle panel shows the cross-correlation function where no obvious correlation is observed. The right one shows the X-ray spectra of the ObsID for hard and soft regions of the lightcurve (upper) and the ratio of the hard and soft spectra (lower), where no obvious pivoting is shown.

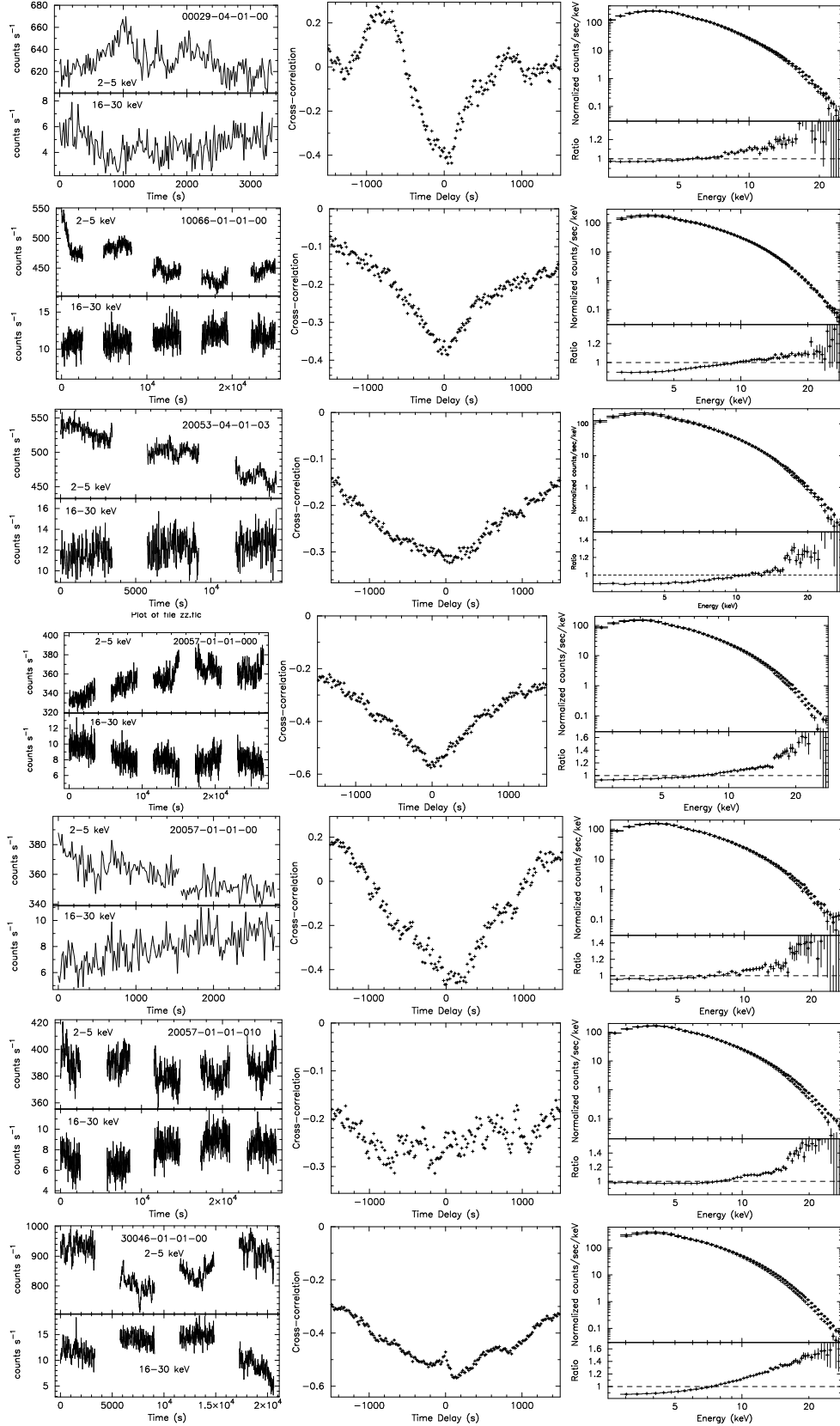


Fig. 4.— The lightcurves, cross-correlations between the soft (2-5 keV) and hard (16-30 keV) X-rays, the X-ray spectra of the ObsID for hard and soft regions of the lightcurve are shown.

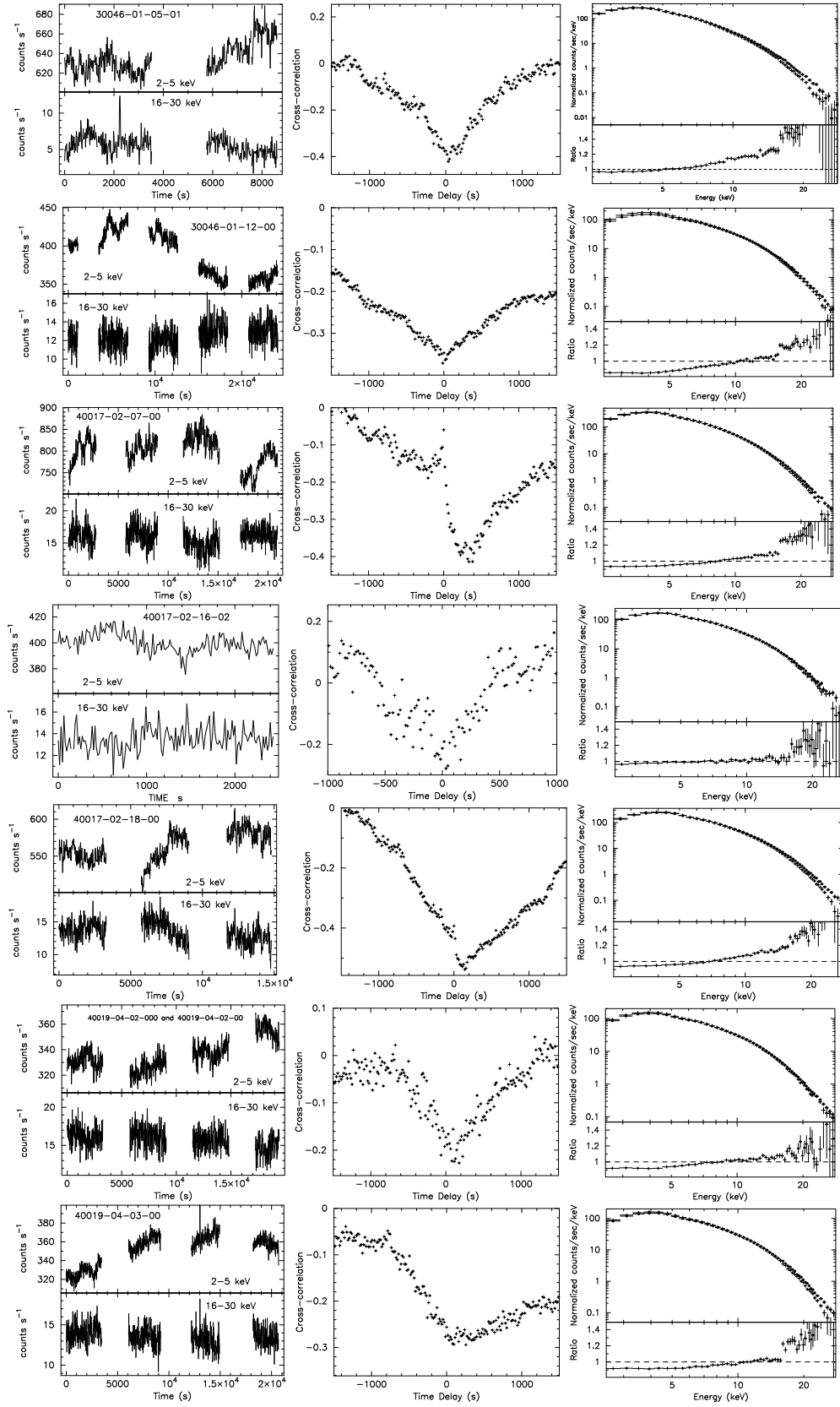


Fig. 4. — Continued.

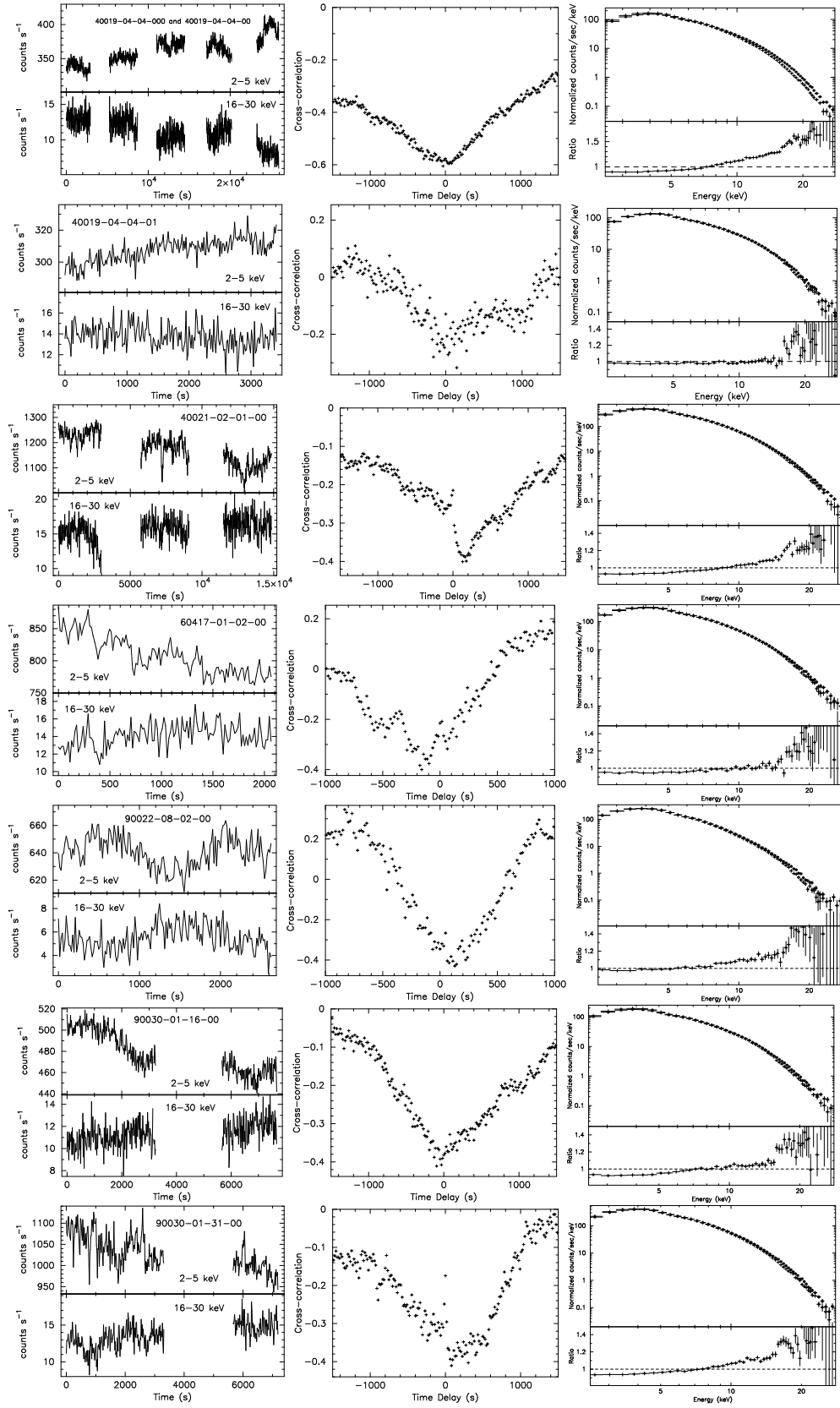


Fig. 4. — Continued

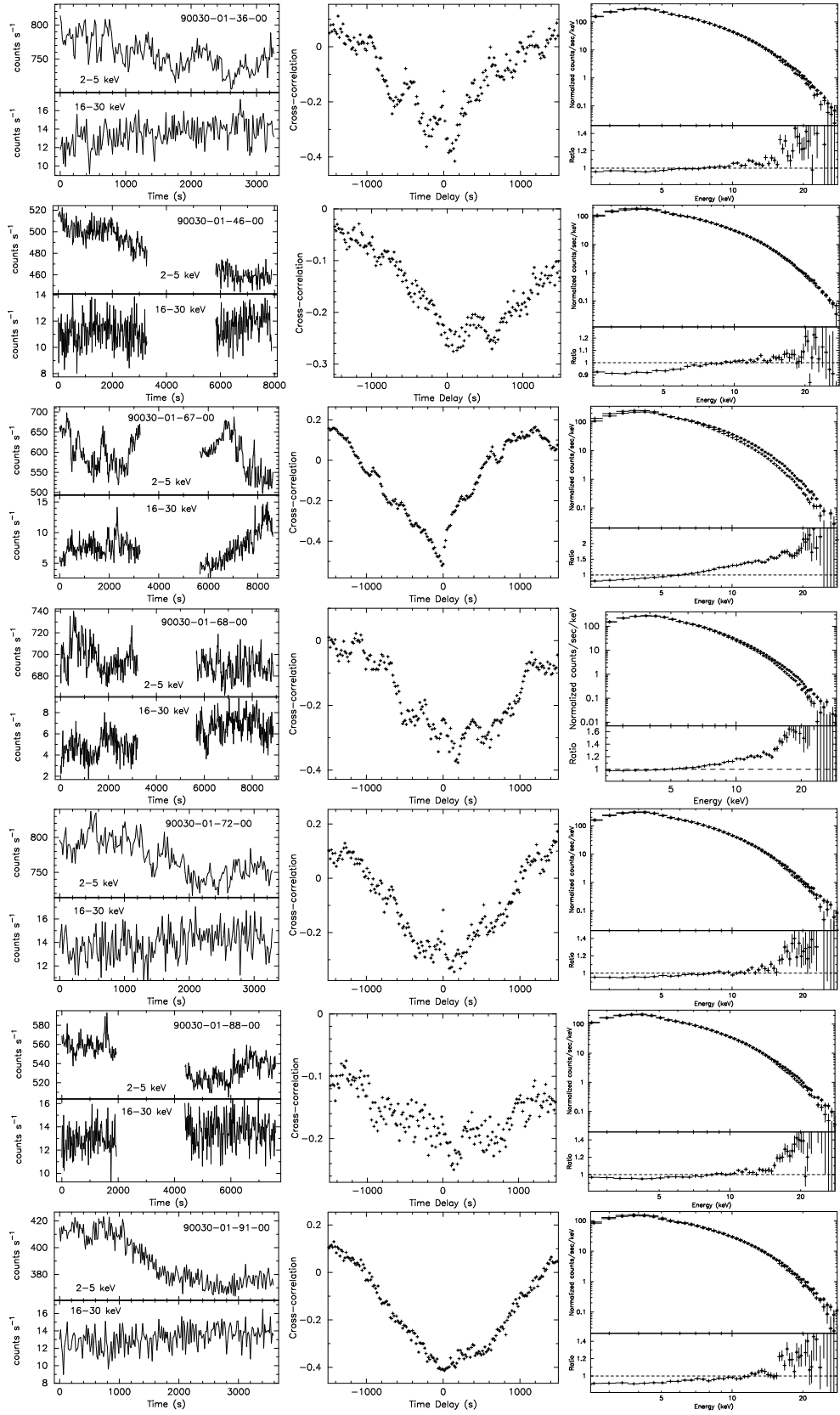


Fig. 4. — Continued

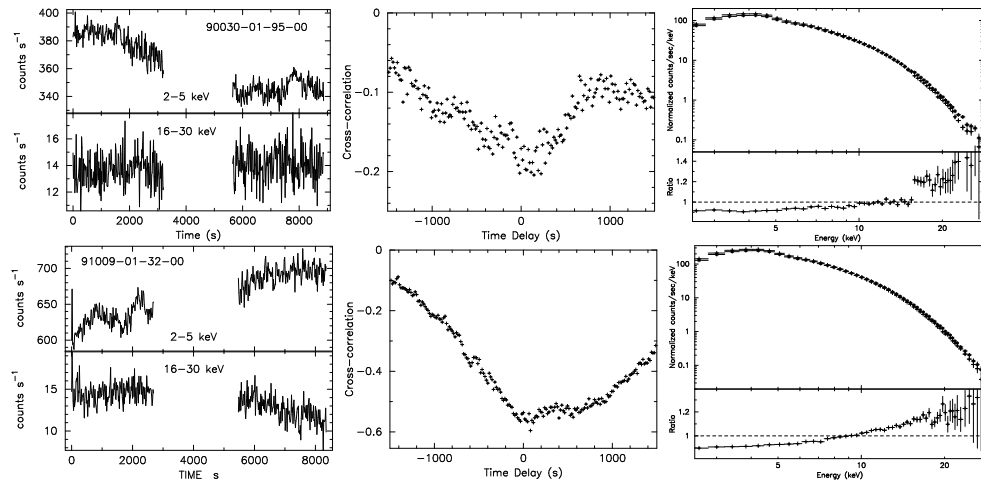


Fig. 4. — Continued

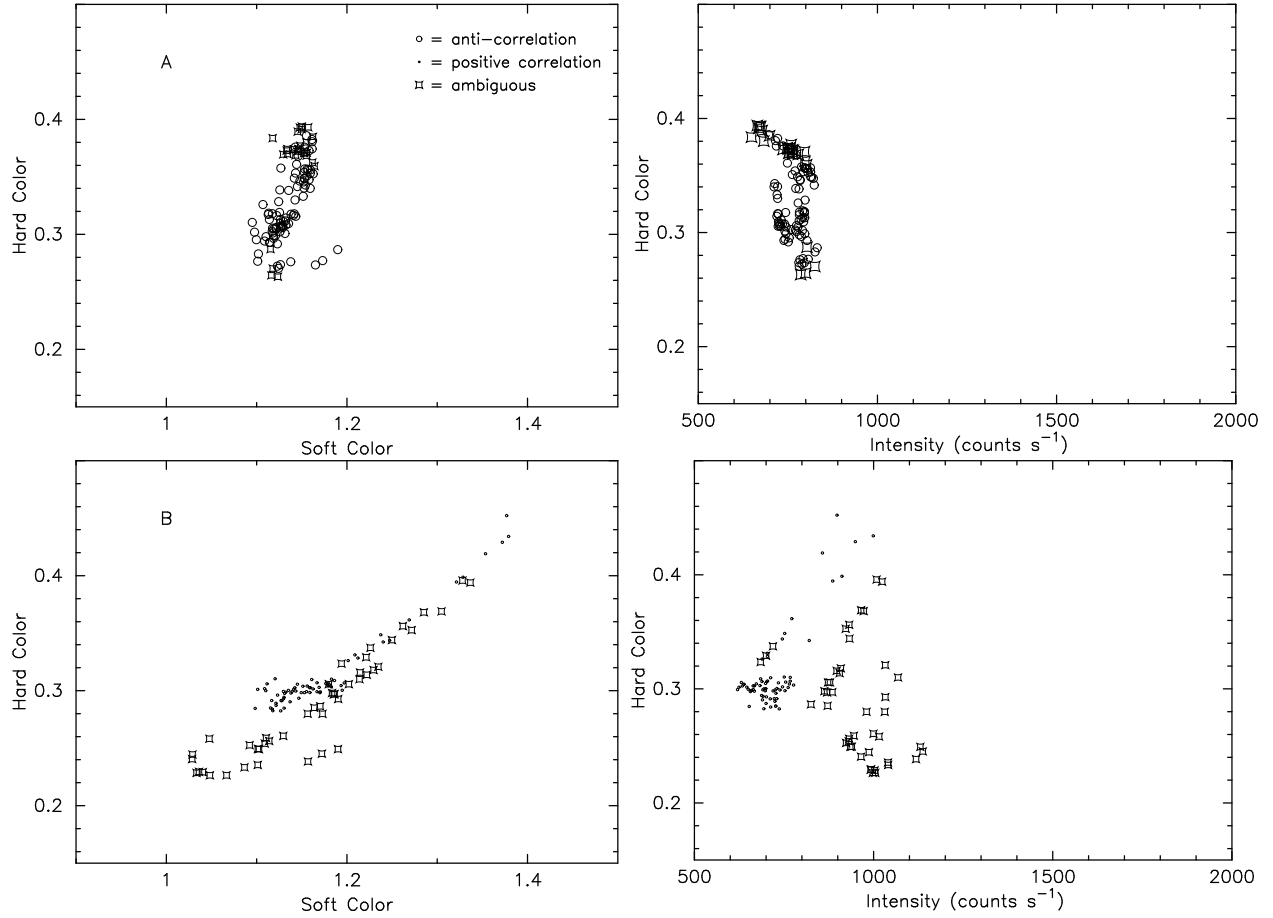


Fig. 5.— The CCDs and HIDs during the low-intensity state from (A) 28/29 September, 1997 and 16/17 December, 1999, (B) 23/24/26 December, 1999. Each point is on average of 1024 s.

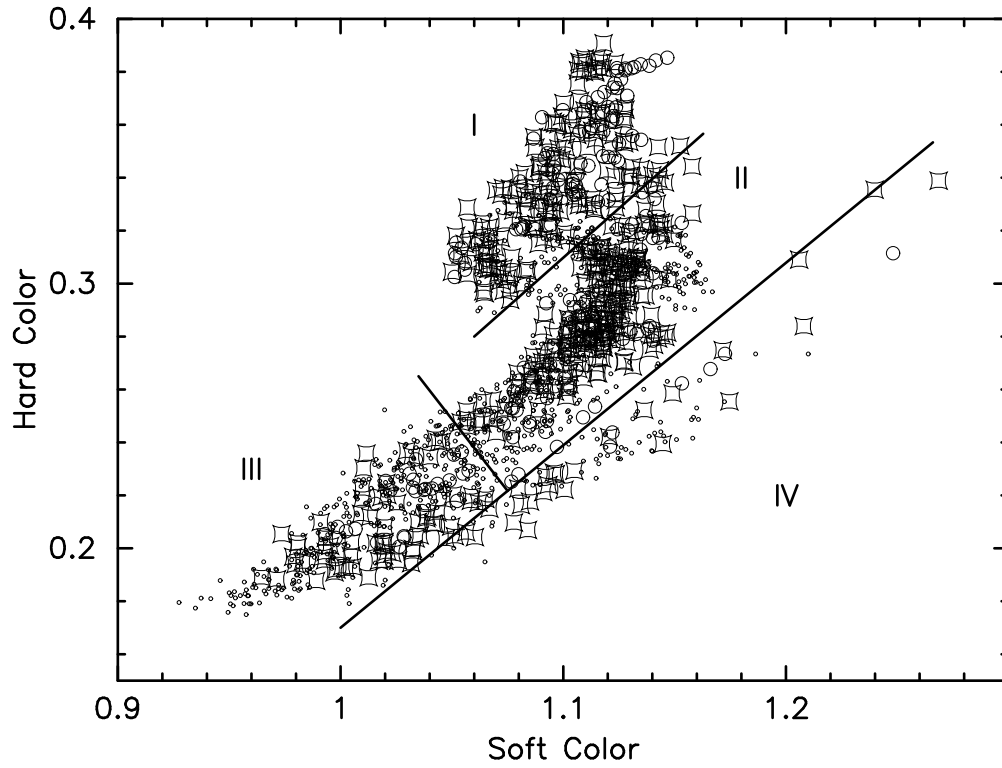


Fig. 6.— The CCD of the observations of the medium-intensity and some low-intensity, which is divided into four regions.

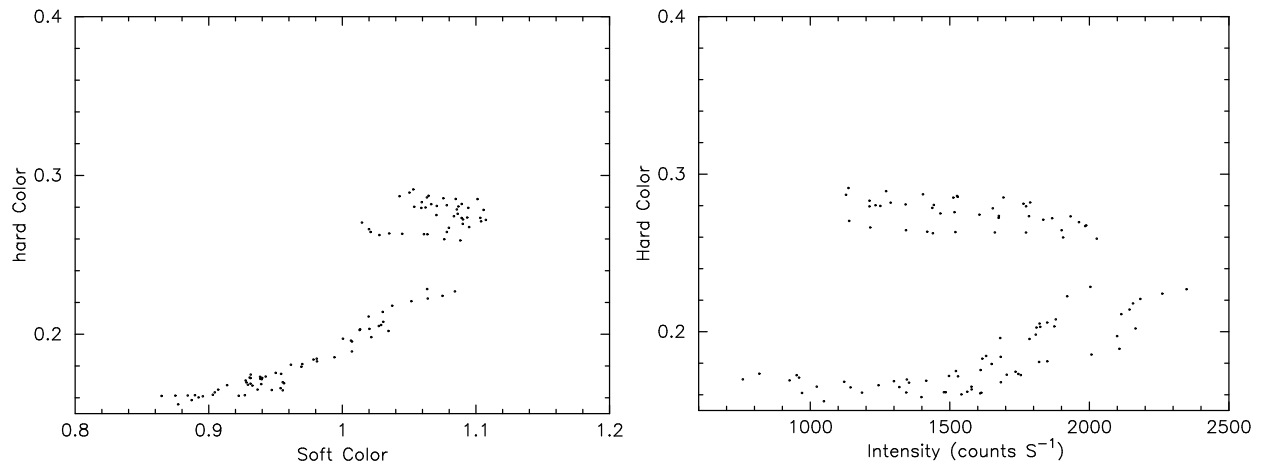


Fig. 7.— The CCD and HID during the high-intensity state of Cyg X-2.